TWENTYFIFTH EUROPEAN ROTORCRAFT FORUM

Paper n° G17

Aeroelastic Analysis and Design for On-blade Active Flap

BY

Noboru Kobiki , Eiichi Yamakawa , Yasumichi Hasegawa
ATIC , Japan

Hirohisa Okawa
ISC , Japan

SEPTEMBER 14 - 16 , 1999
ROME
ITALY

ASSOCIAZIONE INDUSTRIE PER L'AEROSPAZIO, I SISTEMI E LA DIFESA
ASSOCIAZIONE ITALIANA DI AERONAUTICA ED ASTRONAUTICA

Aeroelastic Analysis and Design for On-blade Active Flap

Noboru Kobiki , Eiichi Yamakawa , Yasumichi Hasegawa

ATIC (Advanced Technology Institute of Commuter Helicopter, Ltd.)
Kakamigahara City, Gifu Pref., Japan

Hirohisa Okawa

I S C
Kakamigahara City, Gifu Pref., Japan

Abstract

This paper presents the analytical results of the aeroelastic characteristics of the rotor blade with the active flap on a hypothetical rotor.

At first, the geometric parameters of the active flap is decided based on the hub load analysis; the active flap chord length, span length, outboard location are 10%c, 10%R and 80%R, respectively.

The effect on the rotor vibration reduction by the designed active flap is evaluated in the next step. The active flap analytically demonstrates its capability for vibration reduction at 30kt and 120kt level flight conditions.

The stability analysis is performed at last. It is analytically confirmed that the rotor blade with the active flap designed here has no significant flutter problem.

Notation

AF : Active flap
BAF : Flutter coupled between blade bending and AF
BTF : Bending torsion flutter
c : Blade chord length
cg : Center of gravity
Fh : In-plane force = $(Fx^2+Fy^2)^{1/2}$
HM : Hinge moment of AF
Mh : In-plane moment = $(Mx^2+My^2)^{1/2}$
R : Rotor radius

Introduction

There are several active techniques to reduce BVI noise and vibration of helicopters. Among them, active flap becomes very realistic because of not only its effectiveness, but also the recent progress in development of on-blade actuator made of smart materials. Some ambitious organizations have been working very hard in this area to be the first to make it true. (Refs. 1 to 9)

ATIC decided AF as one of the engineering challenges to be studied and activated two primary works; 1) the actuation system for AF by the smart material actuator with the stroke multiplier mechanism (Ref. 10), 2) the aeroelastic analysis for AF to establish the design policy and to evaluate its capability.

This paper describes the latter one summarizing the research work about the analysis for the aeroelastic characteristics of the rotor blade with the active flap configuration.

1. Objectives

The objectives of this paper are to analyze the items below for the hypothetical rotor.

(1) Describe AF design procedure.
(2) Demonstrate the vibration reduction capability of the designed AF.
(3) Stability analysis for the rotor blade with AF on generally assumed structural and operational conditions.

2. Conditions for Analyses

The geometrical property of the hypothetical rotor and the extent of the parametric study are shown here.

Rotor blade geometry

number of blades :	4
radius :	5.8m
chord length :	0.39m
planform :	rectangular

airfoil : AK100D

Rotor operating condition

hover, thrust : 4000 kgf

100% rotor speed : tip speed 210 m/sec

The unsteady aerodynamics is applied all the analyses with the compressibility correction based on the 2D wind tunnel test of the blade airfoil with trailing edge flap supplemented by the CFD code, UG2. The detail is described in Appendix.

3. AF Design

The aims to utilize AF on the helicopter rotor are vibration/BVI noise reduction and rotor performance enhancement. The design policy for AF here is set up to the vibration reduction by generating the sufficient hub load to compensate the vibratory load from each blade of the rotor. This comes from the two reasons;

1) If an AF has the vibration reduction capability, it is predicted that the AF has BVI noise reduction capability. Because the vibration reduction and BVI noise reduction have the same level of the actuation force. (Ref. 2) This is also valid between the vibration reduction and the rotor performance enhancement.(Ref. 1)
2) The direct evaluation can be performed by assuming that the generated hub load by AF on the hover condition represents the effect of AF on the rotor vibration reduction.

During this AF design process, the extent for the parametric study is as follows.

Active flap excitation condition

frequency : 3, 4, 5/rev

amplitude : 1 deg

Active flap geometry

chord length : 10, 15, 20, 25%c

span length : 10, 15, 20%R

3.1 AF chord length

One of the key features for AF sizing is to achieve lower hinge moment of AF because of powerlessness of on-blade AF actuators.(Ref. 10)

One typical analysis result is shown in Fig.1. The 4/rev hub load generated by AF increases in accordance with AF chord length increase, however, the hinge moment also grows as shown in the upper picture of Fig. 1. In order to make it clear the relationship between the 4/rev hub load generated by AF and the hinge moment, the hub loads are rearranged in the form of the load generated by unit hinge moment as shown in the lower picture of Fig. 1.

This indicates that the smaller chord length, the more effective is AF on a point view of the hinge moment. But the smaller chord length makes the more difficulty in the structural design of AF, which also has a large influence on the design of the actuation hardware.

Consequently, AF chord length is selected 10%c by the engineering compromise with the structural design of AF.

3.2 AF spanwise location

The spanwise location of AF should be selected by the consideration for the blade mode shape in order to efficiently generate the excitation force which engages the vibratory load.

Because 1F mode has a large damping and is difficult to be excited, 2F and 3F modes are regarded as the objects to be excited. 2F has its node at 81%R and 3F has its loop at 78% as shown in Fig.2. To avoid node and to make use of loop to efficiently generate the excitation force on the rotor hub by obtaining the sufficient modal deflection, the outboard location of AF is selected 80%R

3.3 AF span length

The AF span length effect on the generated hub load magnitude is almost linearly proportional as shown in Fig. 3. But a long AF span length sometimes has the unpredictable aeroelastic behavior as shown in Fig. 4, where it can be seen that the loads generated by unit hinge moment have their peaks at 20%c unlike those shown in Fig. 1. This may be caused by the coupling between AF and the over-all blade flapping motion whose node is on AF. AF has the opposite sign movement in the flapping direction across this node, which results in the opposite sign hinge moment distribution across the node, then the large part of the hinge moment is canceled out.

Although the shorter AF span length reduces the capability to generate the hub load, this can be compensated by larger AF amplitude.

Based on this discussion, 10%R AF span length is selected.

4. AF Effect on Vibration Reduction

The effect on the rotor vibration reduction by the designed active flap is evaluated here.

The level flight 30kt and 120kt are selected as the evaluation conditions, because, generally, there is the local maximum of the vibration level at about 30kt in the lower speed range. 120kt is selected as a representative of the cruise speed condition.

In order to study the effect of many AF input, a

multicyclic control algorithm (Ref. 6) is utilized here. AF amplitude which is restricted to 1deg in the parametric study of the previous paragraph is set free by the nature of the multicyclic control algorithm.

The vibration reduction effect on 4/rev hub load which is dominant among all the harmonics is shown in Fig. 5. Each component of the 4/rev hub load on AF-on case is normalized by that on the baseline case (AF-off). Although there can be seen an adverse AF effect in Fy on 120kt case, Fz component which is dominant in 4/rev harmonic is reduced in much larger degree on this case. This results in the 4/rev load reduction as a whole.

The designed AF analytically demonstrates its capability for vibration reduction on both the lower and the cruise speed cases. But we would like to notice that although the required AF amplitude calculated here is 4.5deg for 120kt case, it is required 17deg for 30kt, which can not be available by any smart material actuators at present. (Refs. 7 and 10)

5. Flutter Analysis

The stability analyses are performed to evaluate the possibility for several types of flutters for the rotor blade with AF configuration. The schematics of the structural model for analyses is shown in Fig. 6.
The main features of the structural boundary condition are that;

at 70%R : torsion stiffness Kh
rigid in flapwise and chordwise directions
at 75%R : rigid in flapwise and chordwise directions
at 80%R : torsion stiffness Kh
rigid in flapwise and chordwise directions

If there is no notice about the parameters, the all the flutter analyses are performed on the nominal values as below. These values are estimated from AF size selected in the previous paragraph.

AF natural frequency about hinge : 37.7Hz
Chordwise cg position of AF :
18.8mm aft from AF hinge at mid span of AF
Tip weight location : 31.3%c at 97.9%R
Chordwise cg position of AF actuator :
23.3%c at 76.7%R
Rotor control system stiffness : 57,800kgf/m
Rotor speed : 100%

5.1 AF natural frequency about hinge

The most important concern about the flutter for the rotor blade with AF is the control surface flutter caused by the coupling between the blade flapwise bending motion and AF. One of the two primary factors to this flutter is the torsion natural frequency of AF about the hinge, which comprises the inertia and control system stiffness of AF.

The influence of AF natural frequency about the hinge on the flutter characteristics are evaluated as shown in Fig. 7. 7^{th} mode becomes unstable at less than 29Hz where BAF takes place. But all the modes are stable at the nominal frequency 37.7Hz.

Smaller chord length of AF which enables higher natural frequency about the hinge by reducing the inertia is better for stability point of view as well as the AF efficiency stand point as mentioned before.

5.2 Chordwise cg position of AF

The other primary factor to the control surface flutter is the chordwise cg position of AF. This influence is evaluated as shown in Fig. 8. The analysis here is performed at the AF natural frequency 20Hz to impose the most critical condition to the stability among those shown in Fig. 7.

7^{th} mode is on the unstable side at more than 17mm of the cg position aft from the hinge where BAF takes place. But it is confirmed that there is no instability at the nominal AF natural frequency 37.7Hz (not shown here).

5.3 Chordwise cg position of blade

Nowadays aeroacoustically advanced rotor blades are apt to have the tip shape which makes the blade chordwise cg position aft of the quarter chord such as the swept tip. In order to take this tendency into account, the influence of the chordwise cg position of the blade on the flutter is evaluated as shown in Fig. 9. In this analysis, the blade cg travel is represented by the chordwise tip weight cg position at 97.9%R. The tip weight cg position 31.3%c is equivalent to the blade cg position 25%c.

Although 4^{th} mode decreases its stability as the tip weight cg position goes afterward, this mode is still on the stable side up to the maximum calculated value of the tip weight cg position 47.8%c.

5.4 Chordwise cg position of AF actuator

Another factor to reduce stability by pushing the blade cg further backward is the chordwise cg position of AF actuator. The influence of AF actuator position is investigated with the most aft tip weight cg position (47.8%c) to impose the critical condition.

Fig. 10 shows that although 4^{th} mode has the least stability at about 35%c of AF actuator cg, this mode is still on the stable side.

5.5 Rotor control system stiffness

The rotor control system stiffness is one of the difficulties to be predicted with sufficient accuracy, but this has the predominant influence on the blade dynamic property in torsion. Therefore, the stability analysis is needed over the wide range of the rotor control system stiffness. In order to impose the adverse condition, the analysis here is also performed with the most aft tip weight cg position (47.8%c).

As shown in Fig. 11, although 4th mode has its minimum stability at the nominal rotor control system stiffness (57,800kgf/m), this mode is still on the stable side.

5.6 Rotor speed

The rotor speed is also a factor to cause the flutter. The margin of the rotor speed for the flutter is evaluated as shown in Fig. 12. In order to impose the adverse condition, the analysis here is also performed with the most aft tip weight cg position (47.8%c).

4th mode enters the unstable side at more than 106% rotor speed where BTF takes place. But it is confirmed that there is no instability up to 120% rotor speed at the nominal tip weight cg position 31.3%c (not shown here).

6. Conclusions

1. The geometric parameters of AF are decided analytically based on the hinge moment, blade mode shape and the coupled blade-AF aeroelastic property.

2. The above designed AF has the sufficient capability to reduce the rotor vibration, which is analytically demonstrated on 30kt and 120kt level flight conditions.

3. The stability evaluation for the flutter is carried out for the rotor blade with AF configuration. It is concluded that the rotor with AF designed here has no serious flutter problem on various structural and operational conditions.

Acknowledgments

The authors gratefully acknowledge Mr. Katayama for the contribution to construct the structural input for the hypothetical rotor which is the base for all the analyses presented in this paper.

References

1. Dawson, S., Booth, E., Straub, F., Hassan, A., Tadghighi, H., Kelly, H., "Wind Tunnel Test of an Active Flap Rotor BVI Noise and Vibration Reduction", Proceeding of 51st American Helicopter Society, Fort Worth, TX, U.S.A., May, 1995.
2. Charles, B., Tadghighi, H., Hassan, A., "Higher Harmonic Actuation of Trailing-Edge Flaps for Rotor BVI Noise Control", Proceeding of 52nd American Helicopter Society, Washington D.C., U.S.A., June, 1996.
3. Straub, F., Hassan. A., "Aeromechanic Considerations in the Design of a Rotor with Smart Material Actuated Trailing Edge Flaps", Proceeding of 52nd American Helicopter Society, Washington D.C., U.S.A., June, 1996.
4. Milgram, J., Chopra, I., Straub, F., "A Comprehensive Rotorcraft Aeroelastic Analysis with Trailing Edge Flap Model: Validation with Experimentation Data", Proceeding of 52nd American Helicopter Society, Washington D.C., U.S.A., June, 1996.
5. Fulton, M., Ormiston, R., "Hover Testing of a Small-Scale Rotor with On-blade Elevons", Proceeding of 53rd American Helicopter Society, Virginia Beach, VA, U.S.A., April, 1997.
6. Milgram, J., Chopra, I., "Dynamic of an Actively Controlled Plain Trailing Edge Flap System for a Modern bearingless Rotor", Proceeding of 23rd European Rotorcraft Forum, Dresden, Germany, September, 1997.
7. Schimke, D., Jaenker, P., Wendt, V., Junker, B., "Wind Tunnel Evaluation of a Full Scale Piezoelectric Flap Control Unit", Proceeding of 24th European Rotorcraft Forum paper No. TE02, Marseille, France, September, 1998.
8. Straub, F., Charles, B., "Comprehensive Modeling of Rotors with Trailing Edge Flaps", Proceeding of 55th American Helicopter Society, Montreal, Canada, May, 1999.
9. Friedmann, P., "Rotary-Wing Aeroelastic Scaling and Its Application to Adaptive Materials Based Actuation", Proceeding of 24th European Rotorcraft Forum paper No. DY08, Marseille, France, September, 1998.
10. Hongu,T., Sato, M., Yamakawa, E., "Elementary Studies of Active Flap Control with Smart Material Actuators", Proceeding of 25th European Rotorcraft Forum, Rome, Italy, September, 1999.
11. Hariharan, N., and Leishman, J.G., "Unsteady Aerodynamics of a Flapped Airfoil in Subsonic Flow by Indicial Concepts," Proceedings of the 36th AIAA/ASME/ASCE/AHS/ASC Structures, Structural Dynamics, and Materials Conference, New Orleans, LA, Apr 1995.

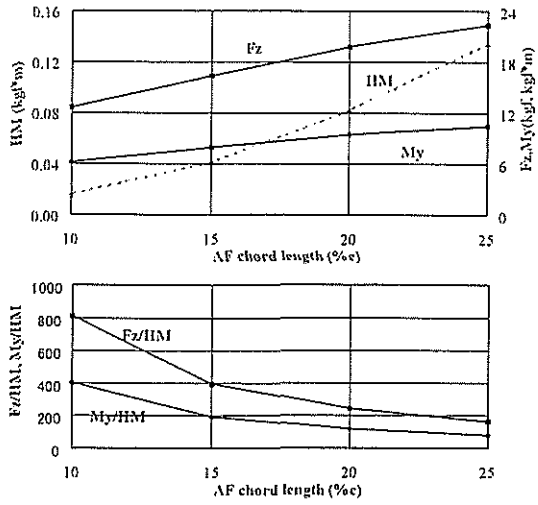

Fig. 1 AF chord length effect on 4/rev hub load
4/rev AF frequency with 1deg amplitude
AF span length 10%R, 70 - 80%R

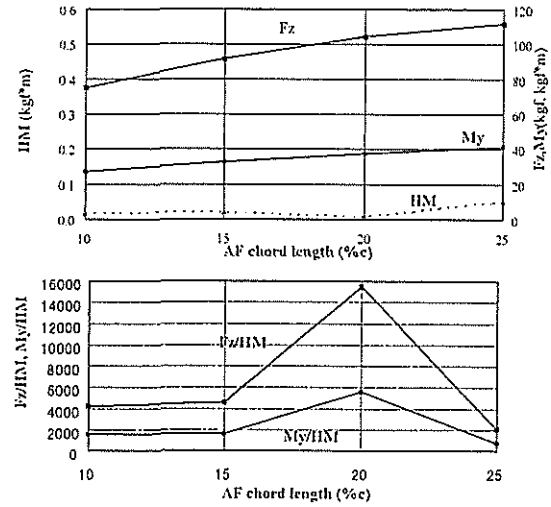

Fig. 4 AF chord length effect on 4/rev hub load
4/rev AF frequency with 1deg amplitude
AF span length 20%R, 60 - 80%R

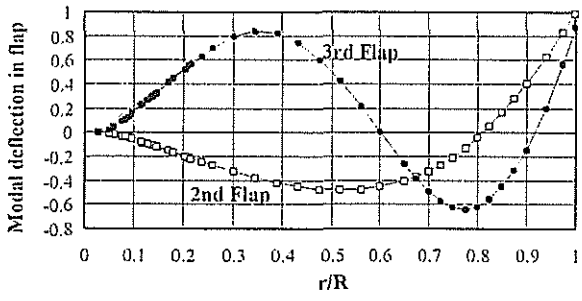

Fig. 2 Mode shape of rotor blade

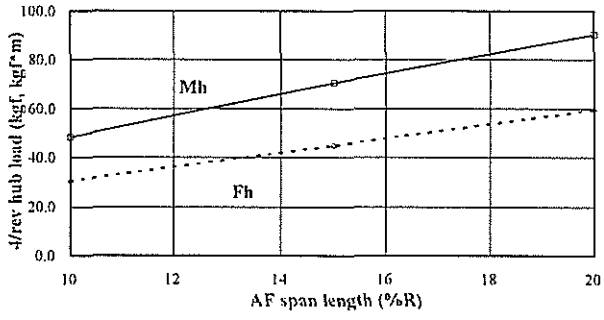

Fig. 3 AF span length effect on 4/rev hub load
4/rev AF frequency with 1deg amplitude
AF span length 10%R, 70 - 80%R

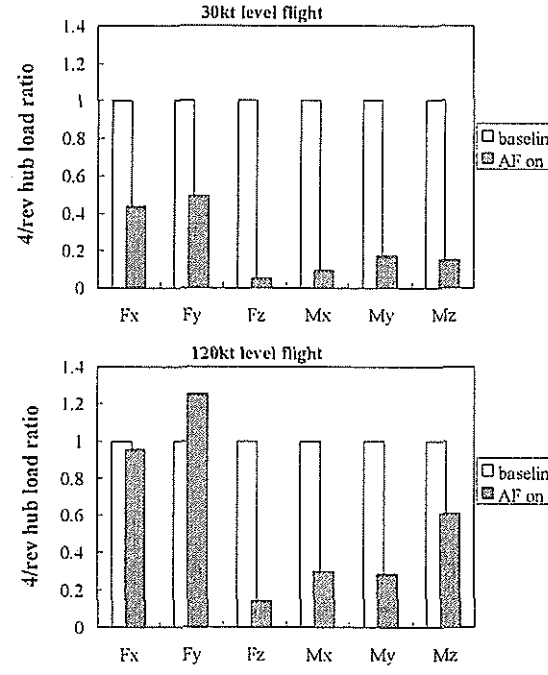

Fig. 5 Designed AF effect on rotor vibration reduction

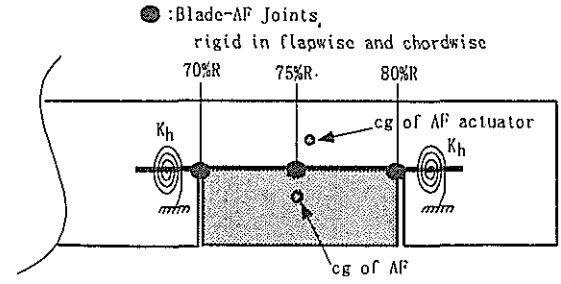

Fig. 6 Structural model for flutter analysis

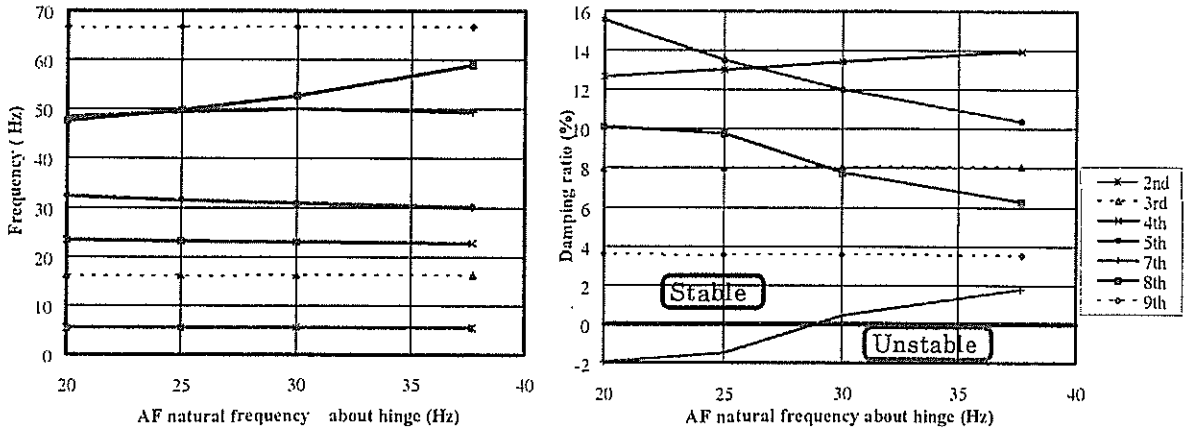

Fig.7 Influence of AF natural frequency about hinge on stability

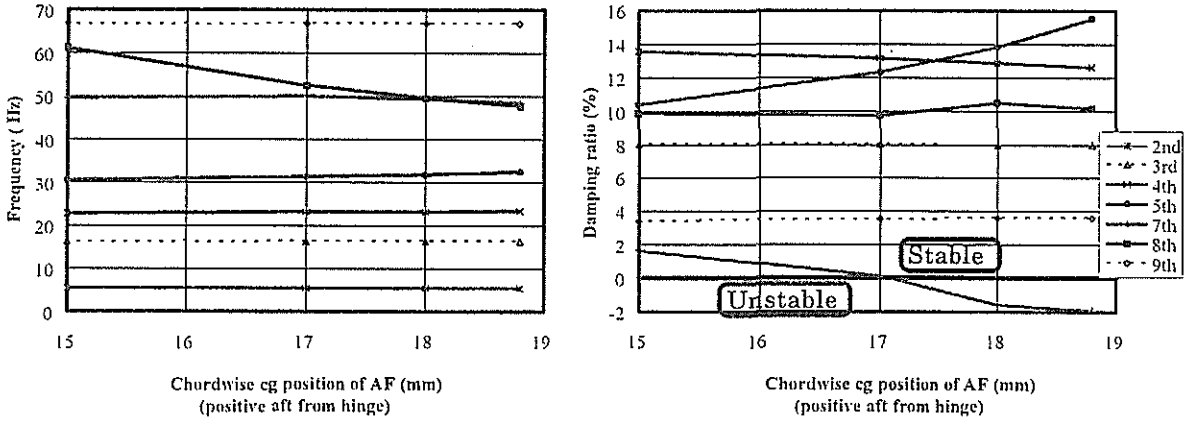

Fig. 8 Influence of chordwise cg position of AF on stability
AF natural frequency about hinge : 20Hz

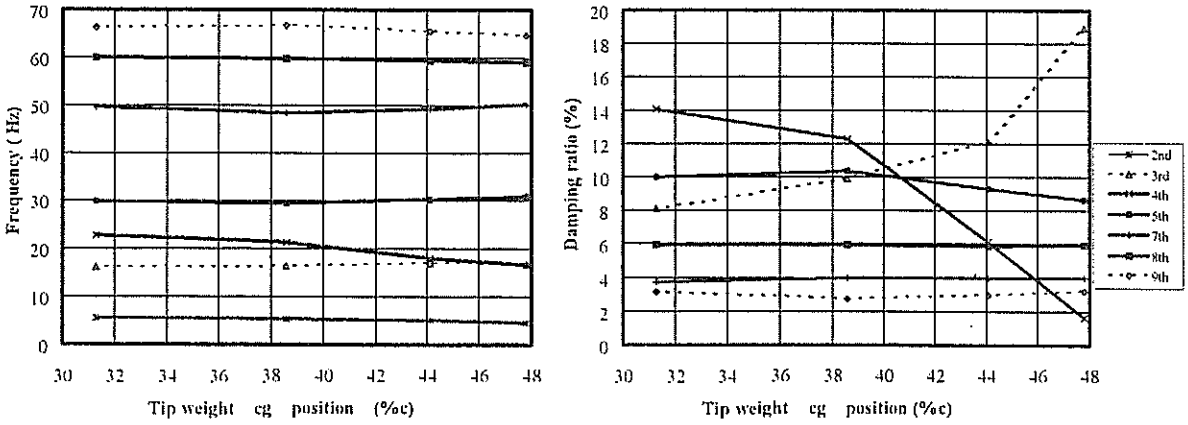

Fig. 9 Influence of chordwise cg position of blade on stability

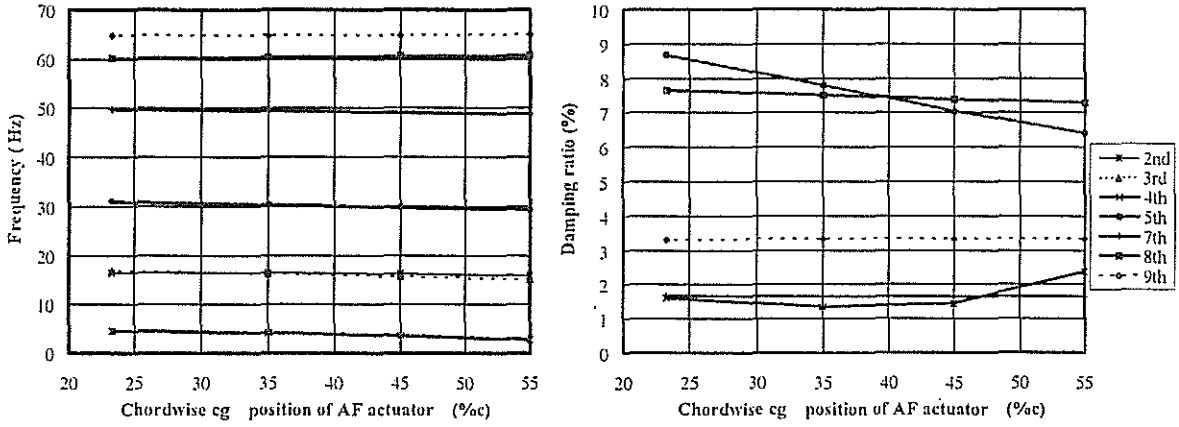

Fig. 10 Influence of chordwise cg position of AF actuator on stability
Tip weight cg position : 47.8%c

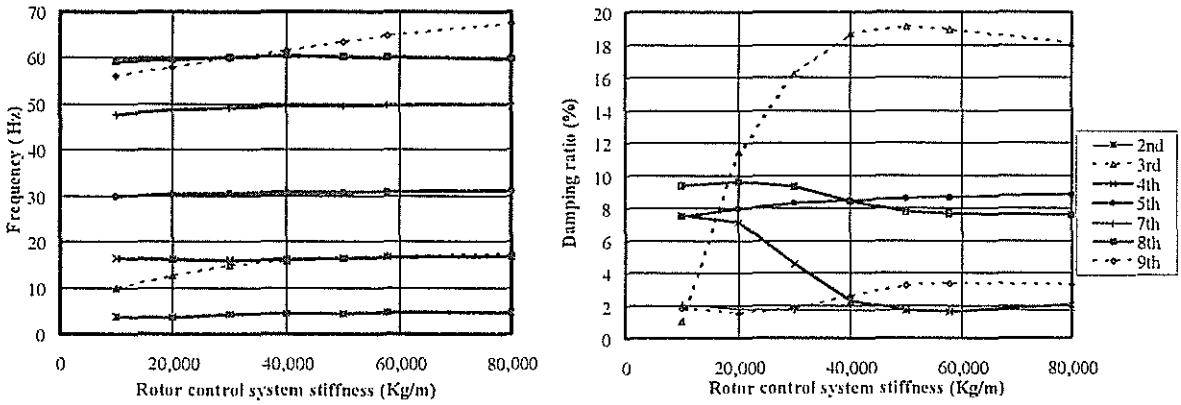

Fig. 11 Influence of rotor control system stiffness on stability
Tip weight cg position : 47.8%c

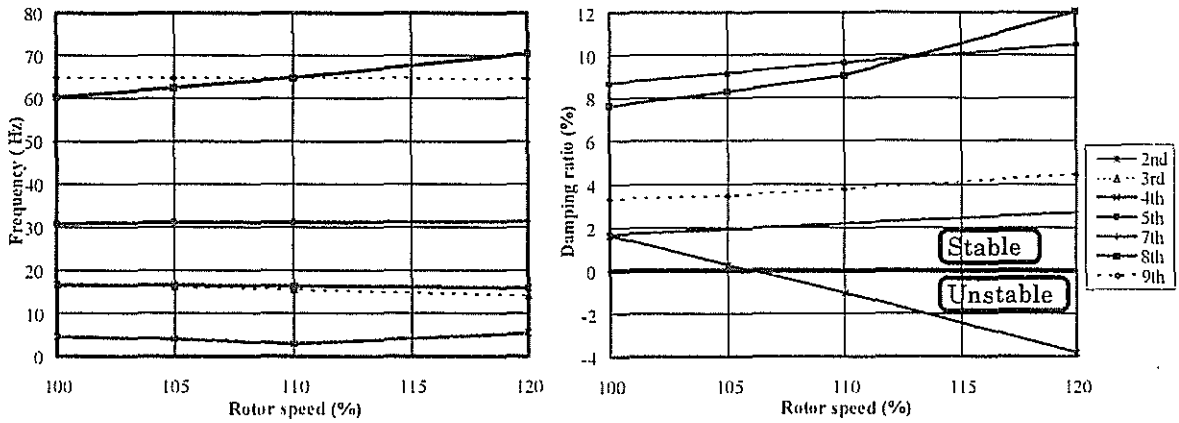

Fig. 12 Influence of rotor speed on stability
Tip weight cg position : 47.8%c

Appendix

Unsteady Aerodynamics for AF Analysis

This section describes the unsteady aerodynamics applied to the analysis in this paper. The incompressible unsteady aerodynamics with the trailing edge flap is formulated at first based on the thin airfoil theory, which contains some revised formulations for those described in Ref. 11. Then, the real airfoil effects such as compressibility and viscosity are taken into account based on the 2D wind tunnel test data of the airfoil with the trailing edge flap. In the last step, the chord length effect of the trailing edge flap is corrected by 2D N-S CFD code, UG2 which is developed in KHI, because the airfoil tested in the wind tunnel has only 25%c trailing edge flap and other chord lengths 20, 15, 10%c are necessary in the parametric study phase for AF design.

1. Incompressible unsteady aerodynamics for airfoil with trailing edge flap

$$C_L = 2\pi C(k)\left[\frac{\dot{h}}{V} + \alpha + b(\frac{1}{2}-a)\frac{\dot{\alpha}}{V}\right] + \frac{1}{V^2}\pi\cdot b\cdot\left[\ddot{h} + V\cdot\dot{\alpha} - a\cdot b\cdot\ddot{\alpha}\right]$$

$$C^f{}_L = \frac{b}{V^2}\left[-V\cdot F_4\cdot\dot{\delta} - b\cdot F_1\cdot\ddot{\delta}\right] + 2\pi C(k)\left[\frac{F_{10}\cdot\delta}{\pi} + \frac{b\cdot F_{11}\cdot\dot{\delta}}{2\pi\cdot V}\right]$$

$$C_G = 2F_{20}\cdot C(k)\left[\frac{\dot{h}}{V} + \alpha + b(\frac{1}{2}-a)\frac{\dot{\alpha}}{V}\right] + \frac{1}{V^2}\left[F_{20} + P_{24} - F_4\right]\cdot V\cdot b\cdot\dot{\alpha} + \frac{1}{V^2}\left[2\cdot F_9\cdot b\cdot\ddot{\alpha} - F_4\cdot\ddot{h}\right]$$

$$C^f{}_G = 2F_{20}\cdot C(k)\left[\frac{F_{10}\cdot\delta}{\pi} + \frac{b\cdot F_{11}\cdot\dot{\delta}}{2\pi\cdot V}\right] + \frac{2}{\pi}P_{21}\cdot\delta + \frac{1}{2V^2}\cdot\frac{2}{\pi}\cdot\left\{P_{21}\cdot(1-e) + P_{25} - \frac{F_5}{2}\right\}\cdot V\cdot b\cdot\dot{\delta} - \frac{1}{2V^2}\cdot\frac{1}{\pi}\cdot F_2\cdot b^2\cdot\ddot{\delta}$$

$$C_M = \frac{1}{2V^2}\pi\cdot\left[a\cdot b\cdot\ddot{h} - (\frac{1}{8}+a^2)\cdot b^2\cdot\ddot{\alpha}\right] + \pi(a+\frac{1}{2})\cdot C(k)\left[\frac{\dot{h}}{V} + \alpha + b(\frac{1}{2}-a)\frac{\dot{\alpha}}{V}\right] - \frac{\pi}{2V^2}(\frac{1}{2}-a)\cdot b\cdot V\cdot\dot{\alpha}$$

$$C^f{}_M = \frac{1}{2V^2}\left[\{F_7 + (e-a)\cdot F_1\}b^2\cdot\ddot{\delta}\right] + \pi(a+\frac{1}{2})\cdot C(k)\left[\frac{F_{10}\cdot\delta}{\pi} + \frac{b\cdot F_{11}\cdot\dot{\delta}}{2\pi\cdot V}\right] - \frac{1}{2V^2}\left[F_{15}\cdot V^2\cdot\delta + F_{16}\cdot V\cdot b\cdot\dot{\delta}\right]$$

$$C_H = -\frac{1}{2}\cdot F_{12}\cdot C(k)\left[\frac{\dot{h}}{V} + \alpha + b(\frac{1}{2}-a)\frac{\dot{\alpha}}{V}\right] - \frac{1}{2V^2}F_{17}\cdot V\cdot b\cdot\dot{\alpha} + \frac{1}{2V^2}\left[-2\cdot F_{13}\cdot b^2\cdot\ddot{\alpha} + F_1\cdot b\cdot\ddot{h}\right]$$

$$C^f{}_H = -\frac{1}{2}\cdot F_{12}\cdot C(k)\left[\frac{F_{10}\cdot\delta}{\pi} + \frac{b\cdot F_{11}\cdot\dot{\delta}}{2\pi\cdot V}\right] - \frac{1}{2\pi}F_{18}\cdot\delta + \frac{1}{2V^2}\left[\frac{1}{2\pi}\cdot F_{19}\cdot V\cdot b\cdot\dot{\delta} + \frac{1}{\pi}\cdot F_3\cdot b^2\cdot\ddot{\delta}\right]$$

The notation is identical to that in Ref. 11 except the followings;

$C_L, C^f{}_L$: identical to C_N and $C^f{}_N$ in Ref.11, respectively

C_G: Flap lift coefficient by airfoil motion, identical to C_F in Ref. 11.

$C^f{}_G$: Flap lift coefficient by flap motion

$$F_3 = -\frac{1}{2} - \frac{1}{8}e^2 + \frac{5}{8}e^4 - (\frac{1}{8}+e^2)\theta_e{}^2 + e\theta_e\sin(\theta_e)\frac{1}{4}(7+2e^2)$$

$$P_{21} = \sin^2(\theta_e) = 1-e^2$$

$$P_{24} = (2-e)\cdot\sin(\theta_e) - \theta_e$$

$$P_{25} = \frac{1}{2}(1-e)\cdot\sin(\theta_e)\cdot(\theta_e - \sin(\theta_e))$$

$$\theta_e = \cos^{-1}e$$

2. Compressibility and viscosity correction

The incompressible unsteady formulation described above is expanded to compressible and viscous form by utilizing 2D wind tunnel test data. Although only C_L and $C^f{}_L$ are presented here in order to save space, the other coefficients can be expanded in the same way.

The equation for C_L is modified to

$$C_L = C(k)\cdot C_{L\alpha}\left[\frac{\dot{h}}{V}+\alpha+b(\frac{C_{L\alpha}}{2\pi}+ac-a)\frac{\dot{\alpha}}{V}\right] + \frac{1}{V^2}\pi\cdot b\cdot\left[\ddot{h}+V\cdot\dot{\alpha}-a\cdot b\cdot\ddot{\alpha}\right]$$

The lift coefficient offset may not be zero in case of asymmetric airfoils. Furthermore, the lift curve slope depends on Mach number and angle of attack. These influences are incorporated as follows;

$$C_L = C(k)\cdot C_l(\beta)+\frac{1}{V^2}\pi\cdot b\cdot\left[\ddot{h}+V\cdot\dot{\alpha}-a\cdot b\cdot\ddot{\alpha}\right]$$

where

$$C_{l\alpha}=\frac{2\pi}{\sqrt{1-M^2}}$$

$$\beta=\frac{\dot{h}}{V}+\alpha+(\frac{C_{l\alpha}}{2\pi}+ac-a)b\frac{\dot{\alpha}}{V}$$

ac: Chordwise position of aerodynamic center

$C_l(\beta)$: 2D lift coefficient based on the wind tunnel data as a function of Mach number and angle of attack

The equation for $C^f{}_L$ is modified in the next. Assuming steady condition, the equation for $C^f{}_L$ becomes;

$$\frac{\partial C^f{}_L}{\partial\delta}=C_{L\alpha}\cdot\frac{F_{10}}{\pi}$$

This equation can be evaluated quantitatively, because $C_{L\alpha}$ and $\frac{\partial C^f{}_L}{\partial\delta}$ are obtained from the wind tunnel test data. But this relationship is not satisfied exactly. To cope with this, the correction factor L_{cor} is introduced as follows;

$$\left.\frac{\partial C^f{}_L}{\partial\delta}\right|_{wind\ tunnel}=L_{cor}\cdot C_{L\alpha}|_{wind\ tunnel}\cdot\frac{F_{10}}{\pi}$$

This correction factor is incorporated as follows;

$$C^f{}_L=\frac{b}{V^2}\left[-V\cdot F_4\cdot\dot{\delta}-b\cdot F_1\cdot\ddot{\delta}\right] + C_{L\alpha}\cdot C(k)\cdot L_{cor}\left[\frac{F_{10}\cdot\delta}{\pi}+\frac{b\cdot F_{11}\cdot\dot{\delta}}{2\pi\cdot V}\right]$$

Summing up C_L and $C^f{}_L$, the total lift is obtained;

$$C_{L\,Total}=C(k)\cdot C_l(\gamma)+\frac{1}{V^2}\pi\cdot b\cdot\left[\ddot{h}+V\cdot\dot{\alpha}-a\cdot b\cdot\ddot{\alpha}\right] + \frac{b}{V^2}\left[-V\cdot F_4\cdot\dot{\delta}-b\cdot F_1\cdot\ddot{\delta}\right]$$

where

$$\gamma=\frac{\dot{h}}{V}+\alpha+(\frac{C_{l\alpha}}{2\pi}+ac-a)b\frac{\dot{\alpha}}{V}+L_{cor}\left[\frac{F_{10}\cdot\delta}{\pi}+\frac{b\cdot F_{11}\cdot\dot{\delta}}{2\pi\cdot V}\right]$$

3. AF chord length correction

The correction factor L_{cor} is calculated here for several AF chord lengths used for the parametric study. As a preparation, $\frac{\partial C^f{}_L}{\partial\delta}$ is calculated with 25%c trailing edge flap configuration to get the correlation between the wind tunnel test data and UG2. Then, the calculation is performed at other flap chord lengths at several Mach numbers as shown in the table below.

$\frac{\partial C^f{}_L}{\partial\delta}$		M		
		0.4	0.55	0.7
c_f/c	25	3.74	3.88	4.32
	20	3.36	3.53	4.24
	15	2.83	2.98	3.53
	10	2.23	2.35	2.80

c_f/c : Flap chord length (%c)

Finally, L_{cor} is obtained from $\frac{\partial C^f{}_L}{\partial\delta}$ as shown in the table below.

L_{cor}		M		
		0.4	0.55	0.7
c_f/c	25	0.94	0.90	0.83
	20	0.94	0.91	0.91
	15	0.90	0.88	0.86
	10	0.86	·0.84	0.83

c_f/c : Flap chord length (%c)